Research Square

Preprints are preliminary reports that have not undergone peer review.
They should not be considered conclusive, used to inform clinical practice,
or referenced by the media as validated information.

Powdered Polysiloxane Resin Infiltrated Low-Density Flexible Ablators

Steven Kim

steven.kim96@utexas.edu

The University of Texas at Austin

Meredith Moore

Koo & Associates International (United States)

Remy Feru

The University of Texas at Austin

Akshar Mashruwala

The University of Texas at Austin

Ben Rech

Koo & Associates International (United States)

Joseph Koo

The University of Texas at Austin

Research Article

Keywords: low-density flexible ablator, polysiloxane resin, thermal protection system, ablation

Posted Date: November 27th, 2026

DOI: https://doi.org/10.21203/rs.3.rs-11719089/v1

License: This work is licensed under a Creative Commons Attribution 4.0 International License.
Read Full License

Additional Declarations: No competing interests reported.

Powdered Polysiloxane Resin Infiltrated Low-Density Flexible Ablators

Steven D. Kim[1*], Meredith Moore[2], Remy Feru[3], Akshar Mashruwala[3], Ben Rech[4], and Joseph H. Koo[5*]

[1]Graduate Research Assistant, Texas Materials Institute, the University of Texas at Austin, Austin, TX 78712, USA
[2]Research Scientist, KAI, LLC, Austin, TX 78739, USA
[3]Graduate Research Assistant, Walker Department of Mechanical Engineering, the University of Texas at Austin, Austin, TX 78712, USA
[4]Lab Manager, KAI, LLC, Austin, TX 78739, USA
[5]Walker Department of Mechanical Engineering, the University of Texas at Austin, Austin, TX 78712, USA

*steven.kim96@utexas.edu & jkoo@mail.utexas.edu

Keywords: low-density flexible ablator, polysiloxane resin, thermal protection system, ablation

Abstract

The development of high-performance ablative materials for thermal protection systems (TPS) has seen increasing demand in the aerospace and defense industries. The present work utilizes the excellent thermal properties of cured polysiloxane resin in its powdered form and the mechanical properties of low-density felt materials to develop a novel family of low-density flexible ablators (LDFAs) suitable for TPS applications where material flexibility and low density are ideal. In this study, the powdered polysiloxane resin is suspended in isopropyl alcohol and homogeneously infiltrated into various felt materials using a vacuum infiltration method. The resulting infiltrated LDFA composites are thoroughly investigated for thermal, flammability, and ablation properties. The LDFAs exhibit excellent flexibility, char structural integrity, and ability to withstand significant heat fluxes.

1. Introduction

Recent increase in interest in space exploration and hypersonic vehicles in both public and private industries has revitalized the development of novel material systems designed to withstand extreme aerothermal conditions. These thermal protection systems (TPS), or heat shields, char and erode during atmospheric re-entry to protect structural components of space vehicles from aerothermal heating [1]. In addition to thermal protection, TPS requires adequate insulating properties to protect internal spacecraft components, as well as minimal weight to reduce the monetary cost of payload launch. TPS materials historically used in spaceflight missions, such as phenolic impregnated carbon ablators (PICA) developed by NASA, have been rigid panels [2]. This made conforming the vital heat shields to mission vehicles difficult and oftentimes required gap fillers to bond multiple tiles together, resulting in the more recent development of conformal PICA (C-PICA) by A. Sidor et al. [3]. Using a near net shape mold combined with liquid composite molding allowed for manufacturing of larger TPS tiles, which reduced part count and allowed

direct installation onto the aeroshell. This newly developed manufacturing method resulted in a new variant of PICA with comparable ablation rate, but C-PICA displays significantly lower thermal diffusivity and remained rigid once de-molded [4]. Apart from the PICA family of TPS materials resulting from phenolic resins, the Koo Research Group (KRG) has explored alternate resin systems for TPS materials. Using 2D carbon fiber (CF) fabric and polysiloxane resin, also known as ultra-high temperature resin, (UHTR), Hou et al. developed a molding compound CF/UHTR composite using a hot melt process [5]. The CF/UHTR composite developed by Hou et al. demonstrated improved moisture resistance, ablation resistance, and thermal stability when compared to MX4926, a CF/phenolic composite. Additionally, work by Yee et al. developed 2D laminate alumina/UHTR composite with varying loadings of boron carbide and found decreased peak back face temperature and low through-the-thickness thermal conductivity [6]. In addition to works by Hou et al. and Yee et al., the KRG at the University of Texas at Austin developed multiple types of novel fiber-reinforced polysiloxane composites (FRPCs) using various fibers infiltrated with UHTR [7]. Fiber substrates studied by the group include glass, silica, carbon, graphite, carbon/polybenzimidazole (C-PBI), alumina, and quartz in different architectures. The FRPCs overall performed favorably against current state-of-the-art phenolic-based material systems when compared under similar aerothermal conditions.

2. Experimental

2.1. Materials

Sourced from Techneglas, LLC, the ultra-high temperature resin (UHTR) 6398-S is a semi-solid colorless resin system formulated using proprietary polysiloxane chemistries to tailor the resin for composites in flame-shielding applications [8-10]. The density and viscosity at 70°C of UHTR 6398-S are 1.2 g/cm³ and 35,000 cPs, respectively. In this study, the polysiloxane resin was b-stage cured and ground down to a fine powder by the Naval Research Laboratory (NRL) to achieve a nominal particle size of 1 μm. This powder was then post-cured at 400°C prior to infiltration to produce powdered UHTR (pUHTR).

Quartzel® quartz needle-punched felts (NPFs) were sourced from Saint-Gobain. Saint-Gobain supplies a wide range of areal weights up to 2,000 g/m² (gsm) [11]. For this study, the 200 gsm and 500 gsm NPFs were selected. Both 200 gsm and 500 gsm NPFs have a nominal density of 0.13 g/cm³.

Along with quartz felts, various carbon-based felts were sourced for this study. VDG and WDF graphitic felts were sourced from Morgan Advanced Materials, and a 60/40 blend of C-PBI felt was sourced from Tex Tech. The VDG and WDF felts have densities of 0.09 g/cm³ while C-PBI has a density of 0.1 g/cm³.

2.2. Infiltration Method

The infiltration procedure used in this study was based on a procedure noted in a patent by Stackpoole et al. and modified to accommodate the UHTR resin [12] better. First, the pUHTR and isopropyl alcohol (IPA) were mixed in a 1:10 ratio using a probe ultrasonicator to form a homogeneous mixture. The felt preforms were prepared as 12.7- x 12.7-cm (5- x 5-inch) squares with a thickness of 2.032 cm (0.8 inch) and placed in a 15.24- x 15.24-cm (6- x 6-inch) steel pan. The prepared UHTR-IPA slurry was poured into the steel pan until the felt was fully submerged.

The steel pan was then placed in a vacuum oven and held under vacuum for 5 minutes at room temperature to allow the powder UHTR to infiltrate into the felt. The infiltrated felt was removed from vacuum and placed in a vented oven at progressively increasing temperatures (70°C, 90°C, 110°C, and 150°C) for 20 minutes each duration, flipping the felt over each time the temperature increased. This ensured that the IPA was fully evaporated. The mass and density of the infiltrated felt were recorded, and the infiltration procedure was repeated until the density reached the 0.3 g/cm³ target. The density of each material was measured using the mass post-infiltration and volume of the felts.

2.3. Fabrication of LDFAs

Following the infiltration method, various felt preforms were infiltrated using pUHTR. Table 1 below summarizes the infiltration results of all felt systems, VDG, WDF, C-PBI, 500Q, and 200Q preforms, compared to the currently used PICA systems. The infiltration cycles taken are denoted via density numbers, and the fiber-to-resin ratio of each composite is shown as well.

Table 1. pUHTR LDFA infiltration results.

Material	Initial Density (g/cm^3)	Density 1 (g/cm^3)	Density 2 (g/cm^3)	Density 3 (g/cm^3)	Density 4 (g/cm^3)	Density 5 (g/cm^3)	Density 6 (g/cm^3)	Density 7 (g/cm^3)	Density 8 (g/cm^3)	Density 9 (g/cm^3)	Fiber: Resin Ratio (wt.%)
VDG/pUHTR	0.085	0.138	0.190	0.276	0.309	-	-	-	-	-	28:72
WDF/pUHTR	0.092	0.141	0.168	0.231	0.352	-	-	-	-	-	26:74
C-PBI/pUHTR	0.109	0.159	0.205	0.252	0.286	0.305	-	-	-	-	36:64
500Q/pUHTR	0.123	0.174	0.263	0.326	-	-	-	-	-	-	38:62
200Q/pUHTR	0.065	0.090	0.134	0.160	0.160	0.185	0.223	0.268	0.321	0.340	19:81
PICA Gen 2	-	0.280	-	-	-	-	-	-	-	-	60:40
PICA Gen 3	-	0.280	-	-	-	-	-	-	-	-	60:40
C-PICA	-	0.330	-	-	-	-	-	-	-	-	73:27

All pUHTR LDFAs were successfully infiltrated to the target density of approximately 0.3 g/cm^3 within three to five cycles, except for 200Q/pUHTR, which required nine infiltration cycles to reach the target density. The LDFA fiber-to-resin ratios range from 19:81 to 38:62. The pUHTR LDFAs are resin-rich, whereas the PICA systems are fiber-rich.

2.4. Characterization Methods

2.4.1. Oxy-acetylene Test Bed

The oxy-acetylene test bed (OTB) setup at the University of Texas at Austin (UT Austin) is equipped with a torch that can output heat fluxes up to 1,600 W/cm^2 to simulate aerothermal ablation conditions of atmospheric re-entry environments. As shown in Figure 1, the OTB is also equipped with a sample holding chuck, back-mounted type-K thermocouples, 2-color IR pyrometer, a camera for in-situ photo/video, and a 2-camera photogrammetry setup. All these components of the OTB allow collection of back-face temperature, front surface temperature, pre- and post-OTB photos, detailed video recording, and photogrammetry analysis. The sample mass is collected before and after ablation along with the sample heights which are measured using a dial depth gauge at the center of the sample ablation crater. The OTB test model is 30 mm

diameter/12.7 mm thick. OTB results are grouped by testing conditions represented by the ablation parameter. Ablation parameter (AP) is defined as the product of heat flux and exposure time, resulting in units of kJ/cm^2 [13]. The pUHTR composites in this study were examined at heat fluxes of 400 W/cm^2 and 600 W/cm^2 for 60 seconds duration, resulting in APs of 24 kJ/cm^2 and 36 kJ/cm^2, respectively, as shown in Table 2. Hereafter, the two OTB test conditions will be denoted as AP24 and AP36.

Table 2. OTB test conditions.

Heat Flux (W/cm^2)	**Exposure Time (s)**	**Ablation Parameter (kJ/cm^2)**
400	60	24
600	60	36

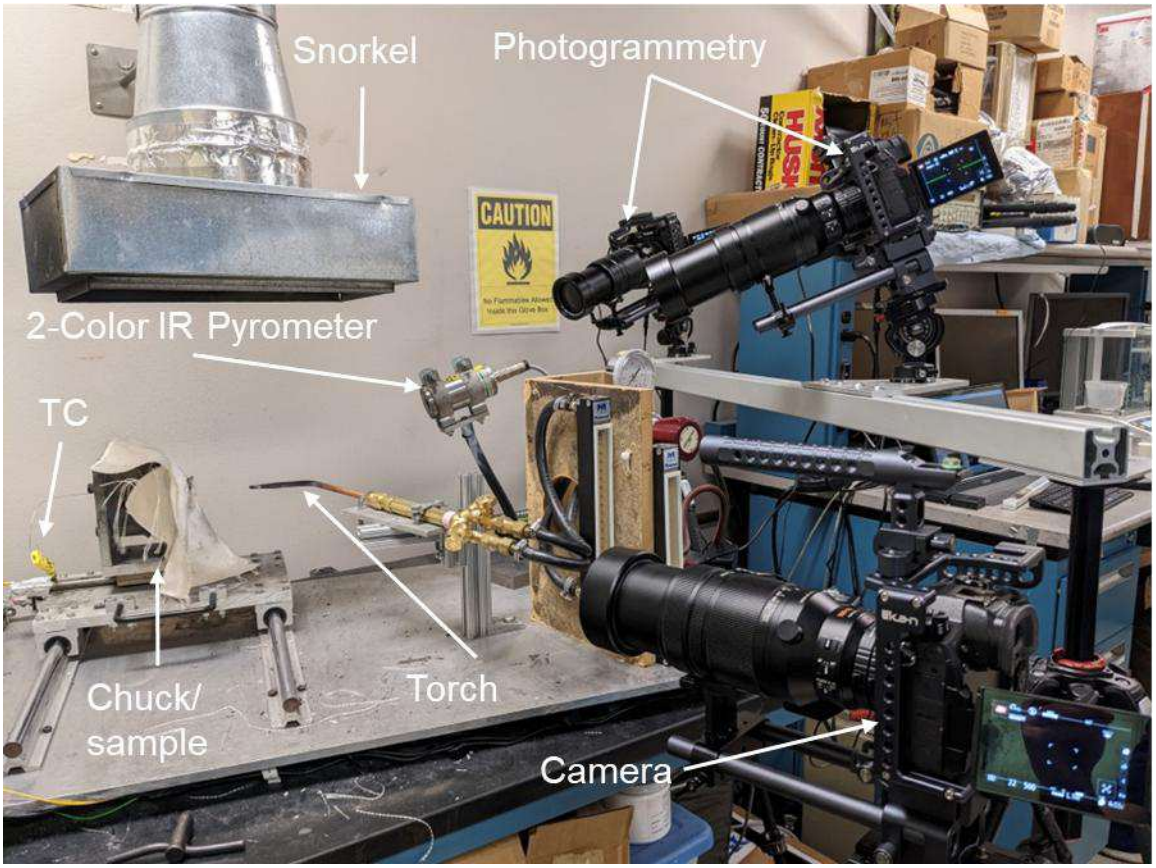

Figure 1. OTB and photogrammetry setup at UT Austin.

2.4.2. Photogrammetry Analysis

Coupled with the OTB system, the 2-camera photogrammetry setup allows for more detailed analysis of the surface morphology of all OTB samples. This non-destructive, visual measurement technique uses stereo-photogrammetric techniques, where a pair of cameras simultaneously capture images of the OTB sample surface during testing. These synchronized image pairs are then

processed to construct 3D point clouds and surface meshes representing the sample surface. The 3D mesh data is compiled and analyzed to generate tabulated data representing overall transient surface behavior and recession [14, 15]. This generated 3D mesh data is then compared to the experimental recession data.

2.4.3. Scanning Electron Microscopy

The Apreo 2C LoVac SEM was used to capture images of all LDFA materials before and after OTB ablation testing to study the surface morphology of each sample. The virgin materials were studied to ensure homogeneous infiltration of the UHTR powder throughout the virgin felt preforms. SEM images of charred samples were observed for char formation and surface morphology of the charred surface.

2.4.4. Bend Radius Test

A bend radius test is conducted to evaluate the ability of the LDFAs to be bent without damage to ensure conformity of the material to a given underlying structure. All pUHTR LDFA composites underwent bend radius tests at increasingly tighter bend radii of 6-, 5-, and 4-inches, and qualitative observations were recorded.

3. Results and Discussion

3.1. Oxy-Acetylene Test Bed Results

Images of pUHTR LDFA composites captured pre- and post-OTB ablation are shown in Figure 2 examined at AP24. None of the samples experienced burn-throughs or torch back-channeling, caused by deep ablation craters, which divert the flame gases back to the torch, causing it to self-extinguish. All AP24 samples withstood the heat flux of 400 W/cm² for the full 60-second test duration.

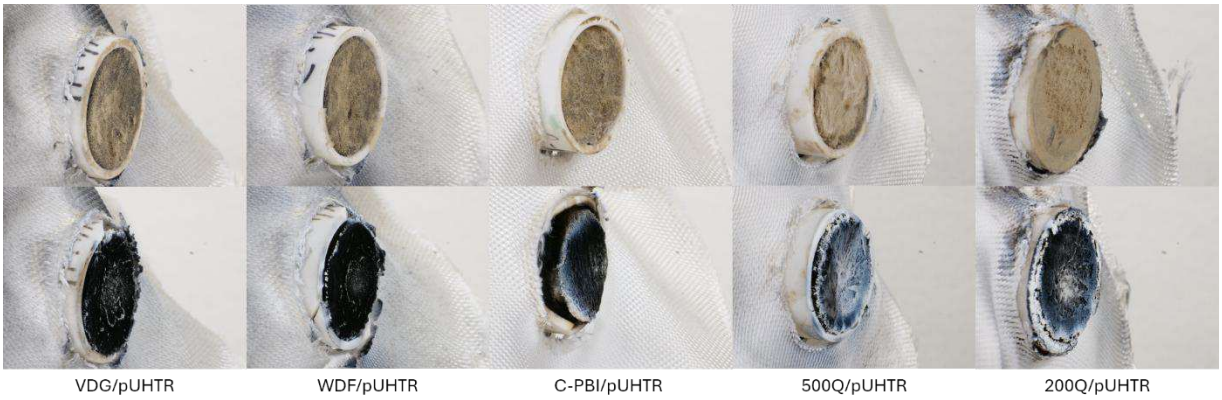

Figure 2. Pre- and post-OTB photos examined at AP 24 kJ/cm^2.

Figure 3 and Figure 4 show summarized OTB data of the pUHTR LDFA composite materials examined at AP of 24 kJ/cm^2. The front surface temperature, recorded using the two-color IR pyrometer, shows the surface temperature at the center of the torch flame's contact area on the sample. A greater front surface temperature signifies a greater amount of heat energy being re-radiated out from the sample surface; therefore, a higher front surface temperature is desirable for

TPS materials. At AP24, as shown in Figure 3, the carbon-based pUHTR composites all display front surface temperatures of 1734°C to 1752°C while the quartz-based pUHTR composites display higher temperatures of 1817°C and 1906°C. This suggests quartz is more effective than carbon or graphite at re-radiating surface heat back into the atmosphere.

Unlike the front surface temperature, the back face heat soak temperature should ideally be low. A lower back face temperature suggests greater effectiveness in the thermal insulative properties of the material as the torch flame heat is conducted through the thickness of the OTB sample. The pUHTR composites show overall improvements in back face heat soak temperature with the exception of C-PBI/pUHTR which showed a large standard deviation. When compared to the PICA control samples, VDG/pUHTR and 500Q/pUHTR displayed greatest improvement in back face heat soak temperatures of 168°C and 194°C, respectively. Amongst the carbon-based pUHTR composites, VDG/, WDF/, and C-PBI/pUHTR, the two graphitic felts, VDG and WDF, significantly outperformed C-PBI. However, the C-PBI/pUHTR resulted in a large standard deviation; therefore, additional trials of this material are necessary to produce more reliable data. Both VDG and WDF samples performed similarly with back face heat soak temperatures of 168°C and 194°C, respectively, both outperforming the PICA control samples at AP24. Between the two composites with quartz substrates, the back face temperature of 500Q/pUHTR peaked at 194°C compared to 333°C of 200Q/pUHTR, a reduction of 42%. This suggests a great correlation between felt areal weight and thermal insulation performance, as 200 gsm quartz felt may not be heavy enough to insulate the underlying structure as effectively as 500 gsm quartz felt. However, despite the underperformance when compared to 500Q/pUHTR, the 200Q/pUHTR sample still outperformed two of the control PICA samples, PICA Gen 2 and PICA Gen 3.

The mass loss rate and recession rate of samples examined at AP24 are shown in Figure 4 below. Overall, the carbon-based pUHTR samples display greater mass loss rates than the quartz-based composites and are comparable to the PICA control samples. The quartz-based pUHTR samples show a mass loss rate of 0.008 g/s for both samples, whereas the carbon-based pUHTR samples all show mass loss rates of 0.012 g/s or greater. The mass loss rate of VDG/pUHTR resulted in a large standard deviation; based on post-ablation photos and in-situ observations, this large deviation is caused by an outlier data point and will likely be greatly reduced with a repeated examination. When compared to the control systems, with average recession rates of 0.076 mm/s to 0.132 mm/s, the pUHTR LDFAs all show greatly reduced average recession rates, ranging from 0.009 mm/s to 0.032 mm/s. Overall, at AP24, the pUHTR LDFAs show promising results with reduced back face heat soak temperatures, mass loss rates, and recession rates.

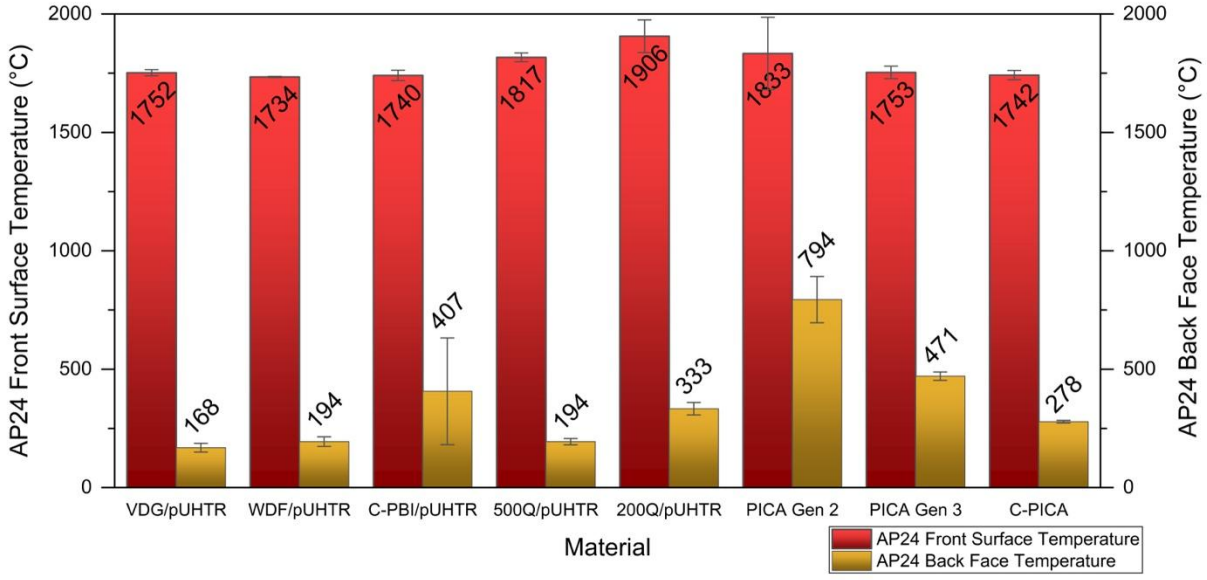

Figure 3. Summarized OTB data of front surface and back face temperatures examined at AP 24 kJ/cm^2.

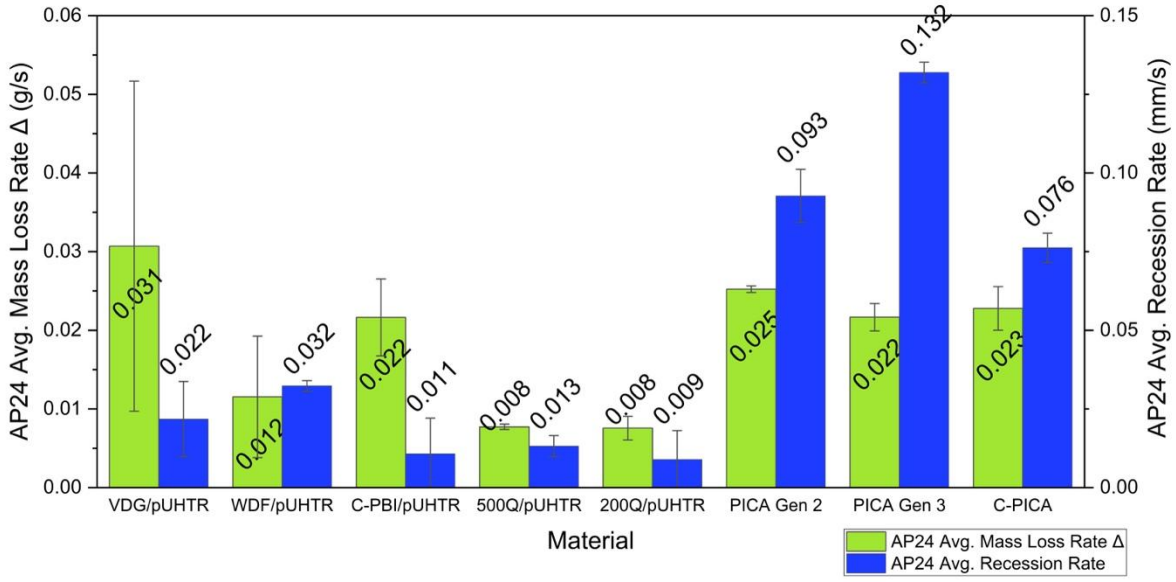

Figure 4. Summarized OTB data of avg. mass loss rate and avg. recession rate examined at AP 24 kJ/cm^2.

The pre- and post-ablation photos of pUHTR LDFA composites examined at AP36, shown in Figure 5 below, exhibit greater recession craters compared to AP24 (Figure 2). At AP36, the samples also did not result in burn-throughs, however, the more aggressive heating environment of 600 W/cm² caused WDF/pUHTR, 500Q/pUHTR, and 200Q/pUHTR samples to develop deep ablation craters which caused the torch flame to back-channel, resulting in premature stops before reaching 60 second durations.

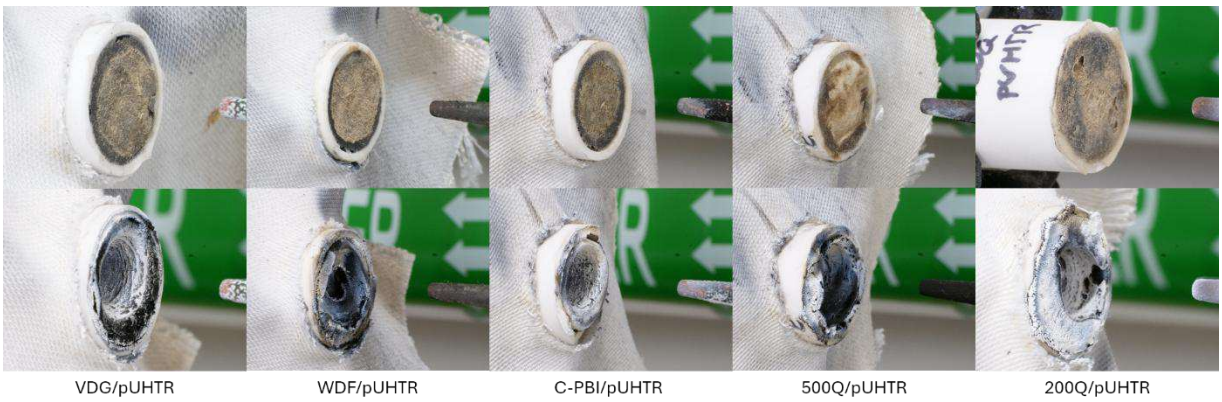

Figure 5. Pre- and post-OTB photos examined at AP 36 kJ/cm^2.

Under the increased aerothermal environment of 600 W/cm² for AP36, all LDFAs exhibited higher front surface and back face temperatures (Figure 6 and Figure 7). Across the board, all AP36 samples resulted in front surface temperatures ranging from 2042°C to 2193°C. Due to the increased recession experienced by WDF/ and 500Q/pUHTR samples, the back face peak heat soak temperatures saw a large increase compared to results in AP24 (Figure 3), resulting in 472°C and 1107°C, respectively. VDG/, C-PBI/, and 200Q/pUHTR samples resulted in lower back face peak heat soak temperatures than PICA Gen 3, however, C-PICA performed exceptionally well at this aerothermal condition, resulting in only 98°C in the back face. Despite the increased AP, VDG/pUHTR remained the best candidate with respect to back face temperature of 224°C.

The average mass loss rate and average recession rate of AP36 (Figure 7) show overall increased mass loss and recession rates compared to AP24 (Figure 4). Despite the overall increase in mass loss rates, VDG/pUHTR resulted in the overall lowest average mass loss rate of 0.013 g/s. WDF/ and 500Q/pUHTR show greatest recession rates of 0.355 mm/s and 0.488 mm/s, respectively. The increased recession rates of these two samples resulted in the formation of deep craters at the torch impingement point and caused back-channeling. These back-channeled samples were aborted early, and the recession rates were calculated based on the premature test durations. The most notable difference between samples examined at AP24 and AP36 is the performance of 500Q/pUHTR. At AP24, the front surface temperature was 1817°C, which is close to the softening point of silica, 1700°C. This resulted in the formation of a stable protective silica melt layer, which aided in the performance of this sample. However, at AP36, 500Q/pUHTR resulted in a much greater front surface temperature of 2101°C, far exceeding the softening point of silica, while experiencing a greater shear force from the torch. This resulted in the silica melt shearing away too quickly before the protective melt layer could properly shield the underlying material – leading to poor performance and back-channeling 29 seconds into the OTB test. A similar phenomenon was seen in 200Q/pUHTR, but to a lesser degree. This difference between 500Q/ and 200Q/pUHTR is likely driven by the much greater resin content of 81 wt.% compared to 62 wt.% of 500Q/pUHTR (Table 1). Silica content is much greater in quartz felt than in UHTR; therefore, this higher UHTR loading in 200Q/pUHTR lessened the effect of the silica melt formation, and the resulting ablation performance was driven by the polysiloxane resin. The

comparatively lower silica content of 200Q/pUHTR assisted in the sample surviving the AP36 test conditions for 59 seconds.

Comparison of recession depths at 24 kJ/cm² and 36 kJ/cm² indicates 36 kJ/cm² is too aggressive of an ablation condition for most pUHTR LDFAs. However, at 24 kJ/cm², all pUHTR LDFAs perform well without experiencing excessive recession depths.

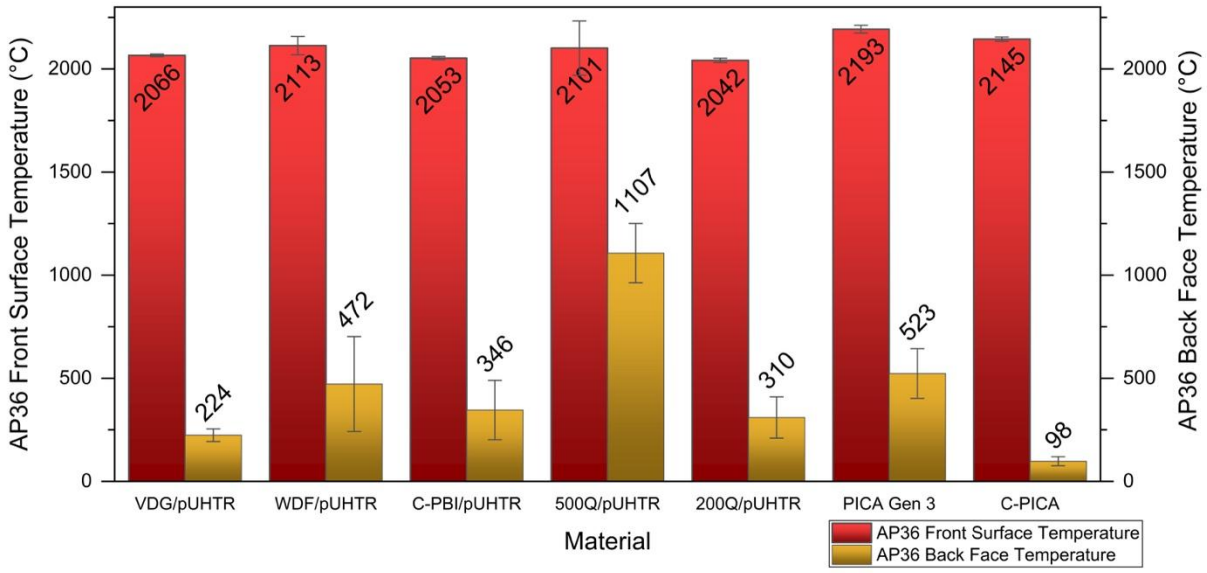

Figure 6. Summarized OTB data of front surface and back face temperatures examined at AP 36 kJ/cm^2.

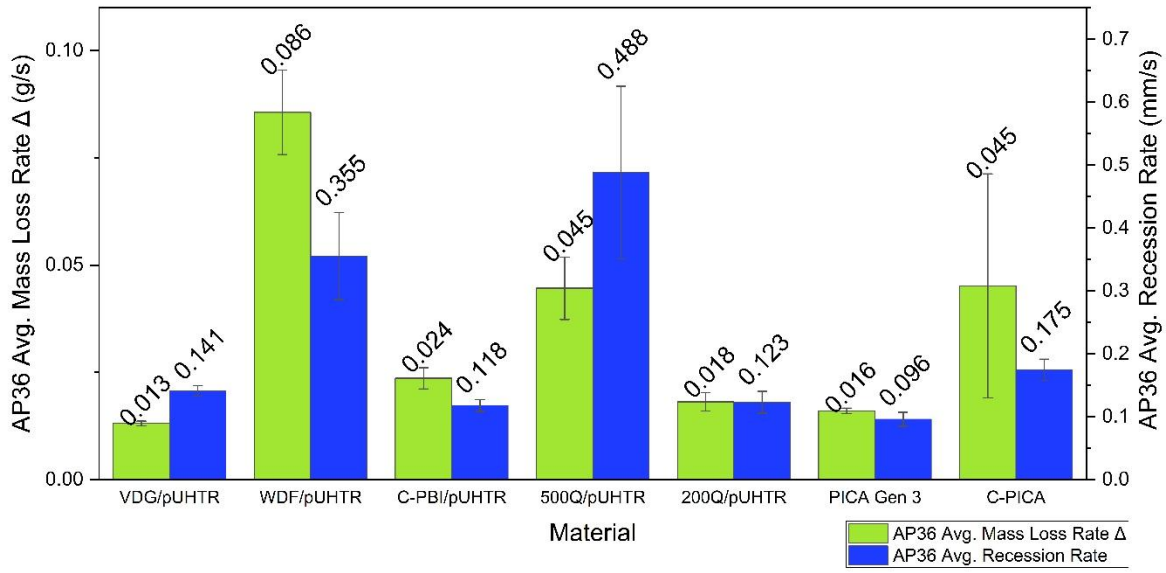

Figure 7. Summarized OTB data of avg. mass loss rate and avg. recession rate examined at AP 36 kJ/cm^2.

3.2. Photogrammetry Results

Photogrammetry data were collected during OTB analysis using the two offset cameras. Figure 8 and Figure 9 summarize the overall surface epicenter recession of pUHTR LDFAs examined at both 24 kJ/cm^2 and 36 kJ/cm^2. At AP 24 kJ/cm^2, VDG/pUHTR experienced the least amount of recession overall, closely followed by WDF/pUHTR. VDG and WDF LDFAs resulted in final recession of 0.74 mm and 0.79 mm, respectively, at the end of the 60-second ablation. The remaining LDFAs, C-PBI, 500Q, and 200Q/pUHTR, recessed at a similar rate; however, the 500Q/pUHTR had a slightly lower final recession of 1.46 mm compared to 1.76 mm of 200Q and C-PBI LDFAs. Compared to the control systems of PICA Gen 3 and C-PICA, all LDFAs exhibited greatly reduced recession and recession rates.

At 36 kJ/cm², the pUHTR LDFA recession rates were significantly higher overall compared to 24 kJ/cm² samples. Due to back-channeling, WDF/, 500Q/, and 200Q/pUHTR samples did not complete the full 60-second OTB test duration. WDF and 500Q samples were aborted at 25 and 29 seconds, respectively, while the 200Q sample lasted for 59 seconds. C-PBI/pUHTR and VDG/pUHTR completed the full 60-second test duration. Due to the premature duration of the WDF/ and 500Q/pUHTR samples, these samples are not directly comparable to the rest of the AP36 recession data. Comparing VDG and C-PBI samples to PICA shows that VDG/pUHTR consistently had lower recession over the duration of the ablation test, while C-PBI resulted in higher recessions overall.

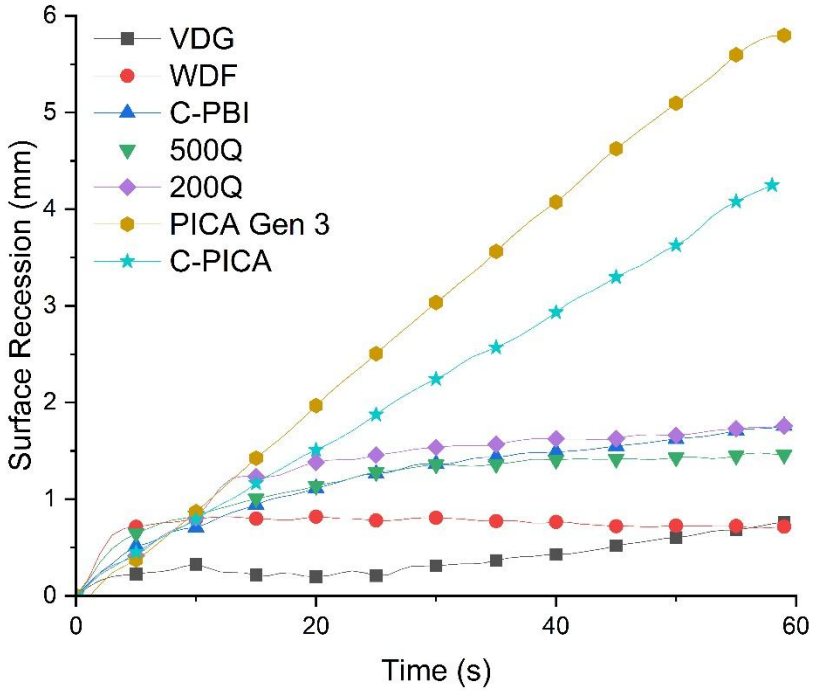

Figure 8. Averaged photogrammetry surface recession of each pUHTR composite examined at AP 24 kJ/cm².

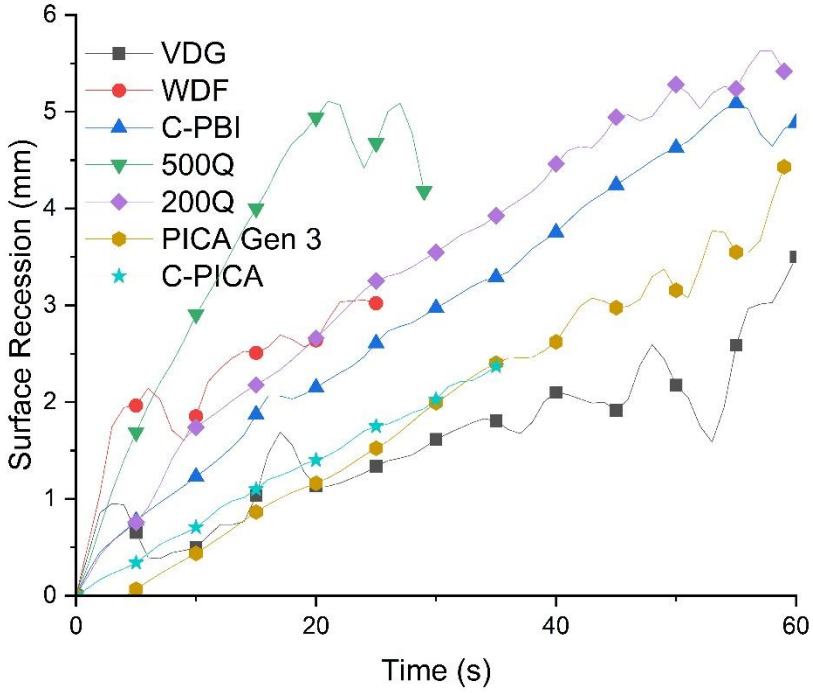

Figure 9. Averaged photogrammetry surface recession of each pUHTR composite examined at AP 36 kJ/cm².

Table 3 and Table 4 below compare the experimental recession data to the in-situ photogrammetry recession data for AP 24 kJ/cm² and AP 36 kJ/cm². The recession rates were calculated by dividing the final recession depth by ablation duration. For both AP24 and AP36, there is a large discrepancy between experimental and photogrammetry recession depths and rates. The validity of the photogrammetry mesh data and recession data was confirmed to be accurate for PICA Gen 2 and PICA Gen 3 [15]. The large error found in the photogrammetry data for the pUHTR LDFAs may be attributed to the lightweight felt architecture of the LDFA composites. Due to the felt substrates not forming a completely solid front surface, the stereo photogrammetry setup could not create a detailed mesh of the surface as the sample ablated, causing the results to not accurately depict the experimental results.

Table 3. Comparison of experimental recession data and photogrammetry recession data examined at AP 24 kJ/cm².

AP24	Experimental Recession		Photogrammetry Recession	
	Final Recession [mm]	Recession Rate [mm/s]	Final Recession [mm]	Linearized Recession Rate [mm/s]
VDG/pUHTR	1.31	0.022	0.74	0.012
WDF/pUHTR	1.94	0.032	0.79	0.013

C-PBI/pUHTR	0.64	0.011	1.76	0.029
500Q/pUHTR	0.79	0.013	1.46	0.024
200Q/pUHTR	0.53	0.009	1.76	0.029
PICA Gen2	5.58	0.093	3.40	0.063
PICA Gen 3	7.00	0.117	5.80	0.104

Table 4. Comparison of experimental recession data and photogrammetry recession data examined at AP 36 kJ/cm².

AP36	Test Duration [s]	Experimental Recession		Photogrammetry Recession	
		Final Recession [mm]	Recession Rate [mm/s]	Final Recession [mm]	Linearized Recession Rate [mm/s]
VDG/pUHTR	60	8.45	0.141	3.50	0.058
WDF/pUHTR	25	8.88	0.355	3.02	0.121
C-PBI/pUHTR	60	7.08	0.118	4.88	0.081
500Q/pUHTR	29	14.16	0.488	4.18	0.144
200Q/pUHTR	59	7.37	0.125	5.42	0.092

3.3. Scanning Electron Microscopy Results

SEM images for each pUHTR LDFA sample pre- and post-OTB ablation at the center of the ablation crater (Figure 10 to Figure 14) were captured to observe changes in the surface morphology of each material due to the effects of surface ablation at AP of 24 kJ/cm². In all pre-OTB photos, the powdered UHTR is found to have coated the fiber substructure of the felt materials, indicating the effectiveness of the pUHTR infiltration method into the felt substrates. The post-OTB SEM images of VDG, WDF, and C-PBI felt systems show the fiber structure remaining after 60 seconds of ablation. These remaining carbon fiber structures are expected to provide structural strength to the charred material. The post-OTB images of 500Q and 200Q quartz felt systems show a silica melt formation rather than the exposed fiber structure. This silica melt formation is caused by the silica present in both the polysiloxane resin and quartz felts melting during direct impingement with the OTB torch flame.

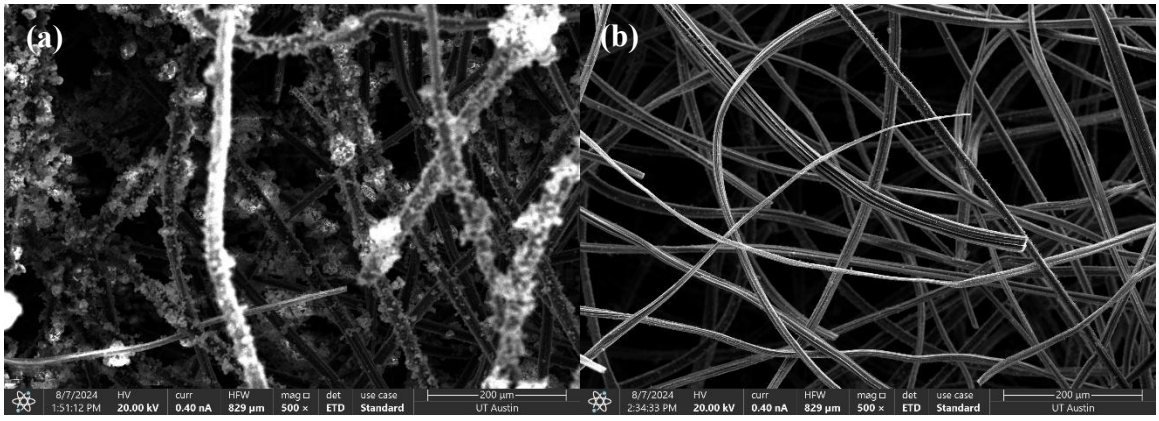

Figure 10. SEM images of VDG/pUHTR (a) pre- and (b) post-OTB at 200 μm scale.

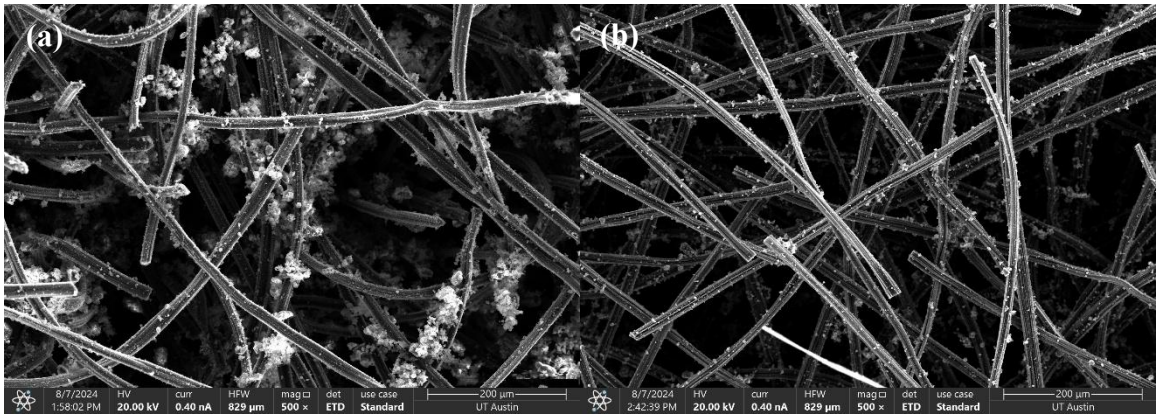

Figure 11. SEM images of WDF/pUHTR (a) pre- and (b) post-OTB at 200 µm scale.

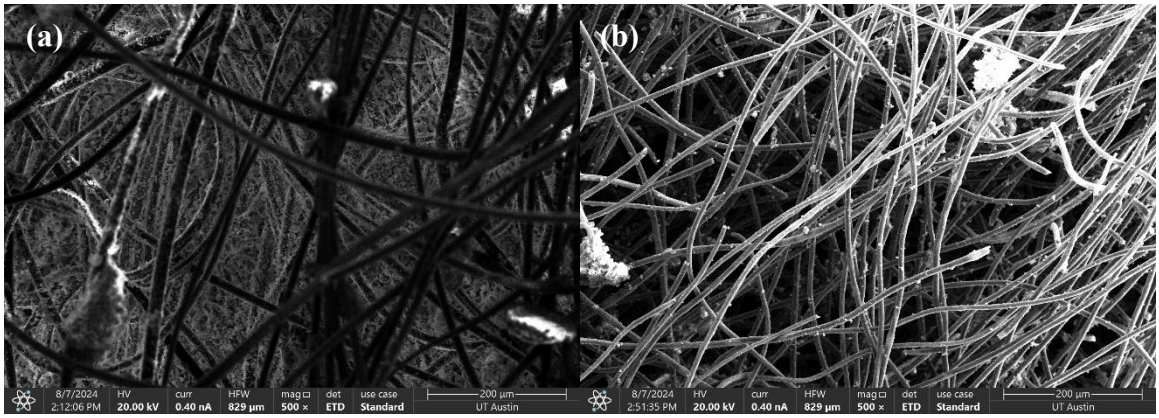

Figure 12. SEM images of C-PBI/pUHTR (a) pre- and (b) post-OTB at 200 µm scale.

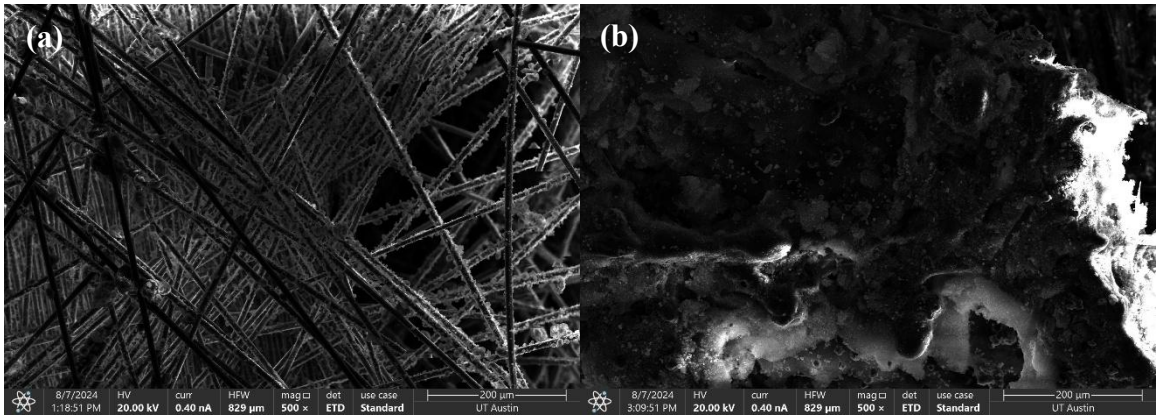

Figure 13. SEM images of 500Q/pUHTR (a) pre- and (b) post-OTB at 200 µm scale.

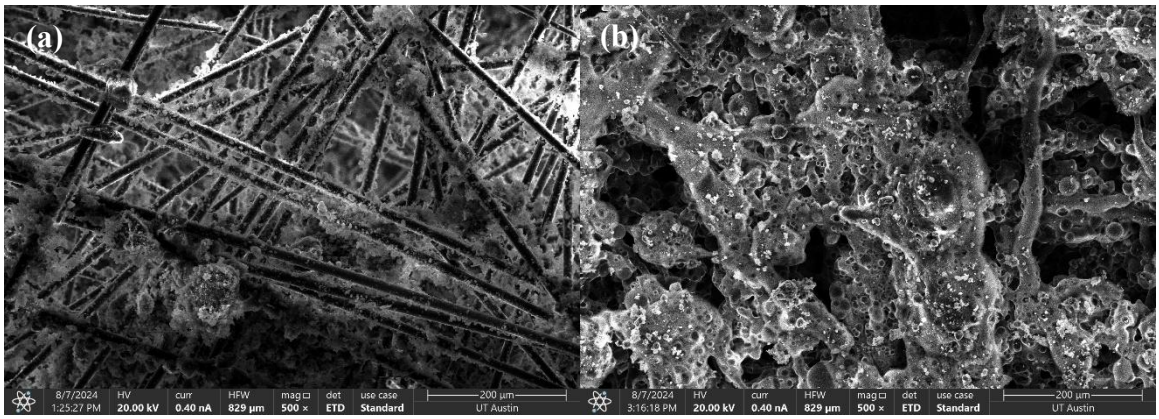

Figure 14. SEM images of 200Q/pUHTR (a) pre- and (b) post-OTB at 200 µm scale.

3.4. Bend Radius Test Results

All pUHTR LDFA composites underwent a bend radius test at increasingly tighter bend radii of 6, 5, and 4 inches. All LDFAs successfully conformed to each of the examined radius and the results of the tightest bend, 4 inches, are shown below Figure 15 to Figure 19. Prior to applying pressure, all LDFAs maintained their rigid shape; however, once downward force was applied by hand to both ends of the material, all LDFAs conformed to the bend radius. After the downward force was released, only VDG/pUHTR returned mostly to its prior shape, while the remaining pUHTR LDFAs remained bent about the bend radius.

The conformity of the pUHTR LDFAs after the felt has been infiltrated with the powdered resin allows great flexibility in the manufacturing and producibility of this material, allowing large-scale infiltrations to occur on flat-shaped felts, and then applied to conical or cylindrical surfaces commonly found on aerospace vehicles. This provides a unique advantage over C-PICA, or conformal PICA, since this variation of PICA requires the felt substrate to be shaped to the desired form before the phenolic resin is impregnated into the felt, forming a rigid material as shown in Figure 20. Therefore, once the C-PICA is formed, its shape cannot be manipulated for other applications.

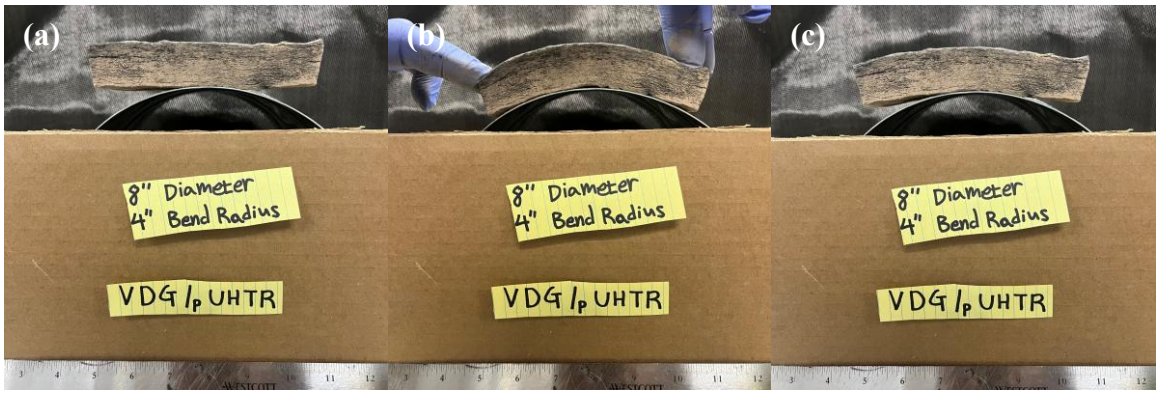

Figure 15. Bend radius test of VDG/pUHTR around a 4-inch radius (a) before, (b) during, and (c) after bend.

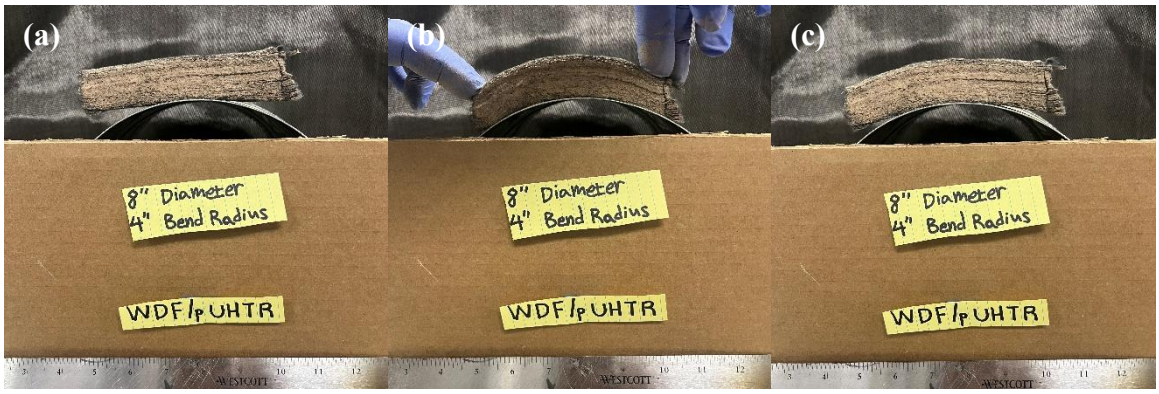

Figure 16. Bend radius test of WDF/pUHTR around a 4-inch radius (a) before, (b) during, and (c) after bend.

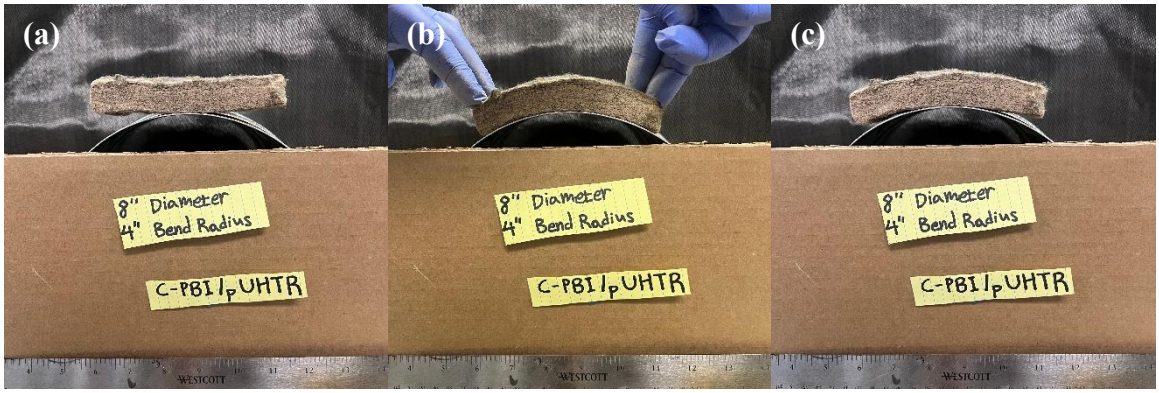

Figure 17. Bend radius test of C-PBI/pUHTR around a 4-inch radius (a) before, (b) during, and (c) after bend.

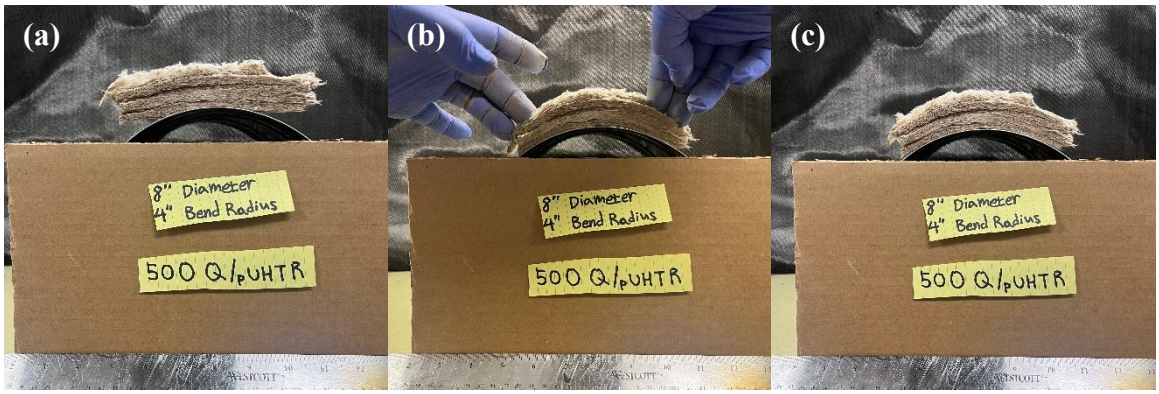

Figure 18. Bend radius test of 500Q/pUHTR around a 4-inch radius (a) before, (b) during, and (c) after bend.

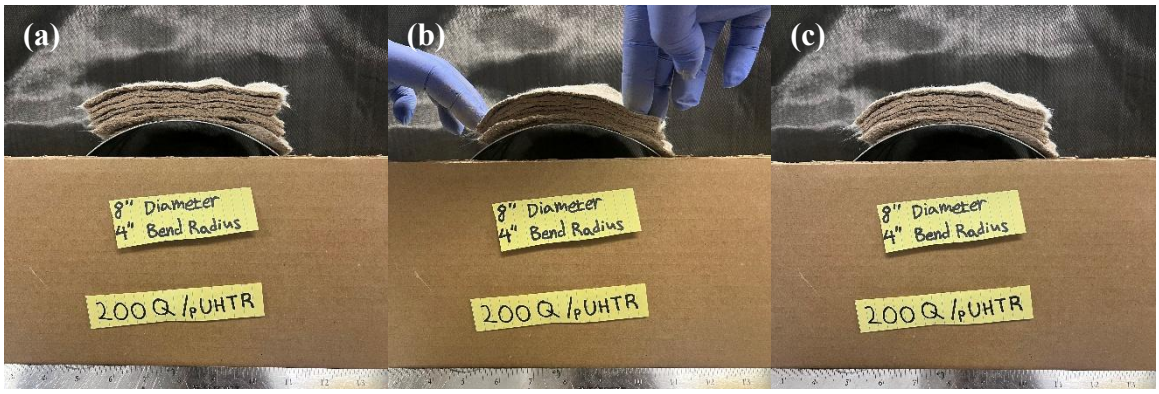

Figure 19. Bend radius test of 200Q/pUHTR around a 4-inch radius (a) before, (b) during, and (c) after bend.

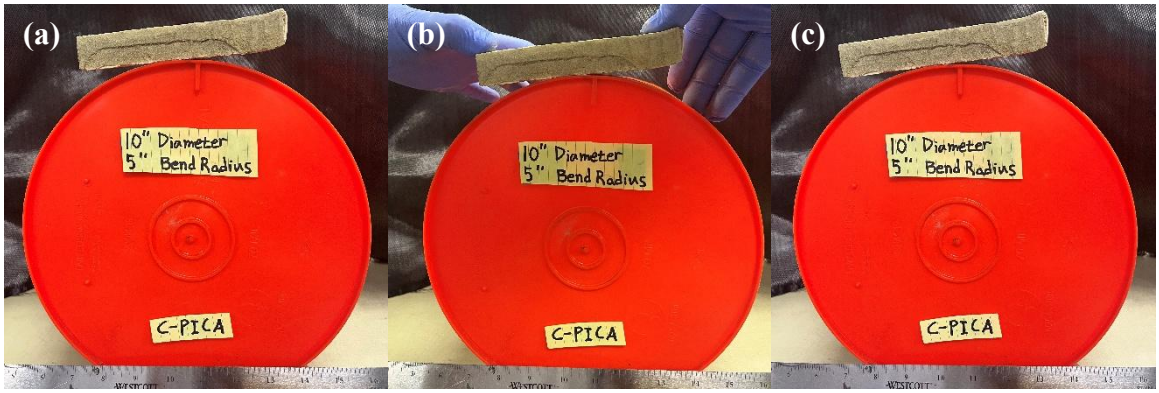

Figure 20. Bend radius test of C-PICA around a 5-inch radius (a) before, (b) during, and (c) after bend.

4. Summary & Conclusions

This study aimed to develop the processing methodology and characterization of LDFA materials by infiltrating powdered UHTR into various felt substrates. In all, VDG, WDF, C-PBI, 500Q, and 200Q felts were infiltrated with pUHTR using vacuum assisted infiltration method to achieve approximately 0.3 g/cm³ density. OTB ablation test models were machined out of the LDFA panels, and OTB analysis was conducted at APs of 24 kJ/cm² and 36 kJ/cm². At low heat flux (400 W/cm^2) AP24 test condition, VDG/pUHTR performed the best in consideration of OTB ablation temperature results. At medium heat flux (600 W/cm^2) AP36 test condition, VDG/pUHTR continued to outperform the other LDFAs to withstand the full 60-second duration at 600 W/cm² with comparatively low mass loss and recession rates. At AP36, WDF/, 500Q/, and 200Q/pUHTR samples failed to complete the full 60-second test duration. For the quartz felt systems, this failure likely resulted from the silica melt shearing away too quickly in the torch flame. The SEM analysis of virgin pUHTR LDFAs samples showed successful infiltration of pUHTR on all felt systems, while post-ablation images showed the remaining fiber structure of carbon fibers and the formation of a silica melt to provide structural integrity. Although photogrammetry analysis of in-situ recession data deviated from experimental values, these data are expected to improve as photogrammetry analysis methods are refined, and the hardware configuration is further developed

with additional cameras to form a more defined 3D mesh of the sample surface. In-situ recession data are most useful to validate material response modeling. All virgin pUHTR LDFAs successfully conformed around the increasingly tighter bend radii of 6, 5, then 4 inches without any damage. Overall, the pUHTR LDFAs exhibit excellent ablation characteristics at low heat flux regimes by providing improved insulative properties but may not be suitable for medium heat flux applications where expected heat flux surpasses 600 W/cm² for extended durations over 30 seconds.

Acknowledgements

Dr. Jarrod Buffy of Techneglas, LLC provided advice on UHTR polysiloxane processing techniques. Dr. Matthew Laskoski's group at the Naval Research Laboratory provided the use of their laboratory equipment to grind and fully cure the powdered polysiloxane resin. The felt materials were supplied by various manufacturers: VDG and WDF graphitic felts by Morgan Advanced Materials, C-PBI felt by Tex Tech, and 200 gsm and 500 gsm needle-punched quartz felts by Eric Smith of Saint-Gobain. PICA Gen 2 and PICA Gen 3 were supplied by Dr. Steve Violette of Fiber Materials Inc. (FMI).

References

[1] Koo JH, Miller MJ, Weispfenning J, Blackmon C. Silicone polymer composites for thermal protection system: fiber reinforcements and microstructures. Journal of Composite Materials. 2011;45(13):1363-80. https://doi.org/10.1177/0021998310381536.

[2] Tran HK, Johnson CE, Rasky DJ, Hui FCL, Hsu M-T, Chen YK. Phenolic Impregnated Carbon Ablators (PICA) for Discovery class missions. AIAA 31st Thermophysics Conference. New Orleans, LA, 1996. https://doi.org/10.2514/6.1996-1911.

[3] Sidor AT, Braun RD, Beck RA, Stackpoole MM. Vacuum Infusion Process Development for Conformal Ablative Thermal Protection System Materials. AIAA SciTech. Orlando, FL, 2017. https://doi.org/10.2514/6.2017-5199.

[4] Milos FS, Gasch M. Conformal Phenolic Impregnated Carbon Ablator (C-PICA) Arcjet Testing, Ablation and Thermal Response. AIAA SciTech. Kissimmee, FL, 2015. https://doi.org/10.2514/6.2015-1448.

[5] Hou Y, Yee C, Li W, Koo JH, Li L, Rech B, et al. A novel ablative material for thermal protection system: Carbon fiber/polysiloxane composites. Aerospace Science and Technology. 2022;129:107822. https://doi.org/10.1016/j.ast.2022.107822.

[6] Yee CM. Development, Manufacturing, Characterization, and Modeling of a Novel Alumina/Polysiloxane/Boron Carbide Ablative Composite. AIAA SciTech. Orlando, FL, 2025. https://doi.org/10.2514/6.2025-0572.

[7] Koo JH, Hou Y, Yee C, Kim SD, Bernstein S, Feru R, et al. Novel Fiber-Reinforced Polysiloxane Composites: Processing, Characterization, and Modeling for Hypersonic Applications. Journal of Composites Science. 2026;10(8):382. https://doi.org/10.3390/jcs10080382.

[8] Schellhase KJ, Koo JH, Wu H, Buffy JJ. Experimental Characterization of Material Properties of Novel Silica/Polysiloxane Ablative. Journal of Spacecraft and Rockets. 2018;55(6):1401-13. https://doi.org/10.2514/1.A34044.

[9] Fish C, Buffy J. Burning Bush Group, LLC, High Performance Compositions and Composites. USPTO. 2017.

[10] Fish C. Techneglas, LLC, High Performance Compositions and Composites. USPTO. US010259972B2. 2019.

[11] Smith E. Advances in Quartz Fiber Reinforcements for Composite Applications. SAMPE Journal. 2023;May/June:44-50.

[12] Stackpoole MM, Ghandehari EM, Thornton JJ, Covington MA. Flexible ablators. USPTO. US9592923B1. 2017.

[13] Koo JH, Bernstein S, Pilato L. A Novel Approach to Investigate Thermal Protection Systems Materials. SAMPE Journal. 2024;60(2). https://doi.org/10.33599/SJ.v60no2.03.

[14] Yee CM, Maragoudakis EY, Woo K, Langton N, Joyce TT, Koo JH. Design of a Photogrammetric System for Real Time Surface Morphology Analysis. AIAA SciTech. National Harbor, MD, 2023. https://doi.org/10.2514/6.2023-1538.

[15] Feru RM, Yee C, Rech B, Koo JH. Photogrammetry Methods for Transient Surface Recession Measurement of Materials During Aerothermal Testing. AIAA SciTech. Orlando, FL, 2025. https://doi.org/10.2514/6.2025-0575.